Micro- and macrophase separation in complex polymer systems

Huh, J

Chapter 4

Micro- and Macrophase Separation in Blends of Reversibly Associating One-End-Functionalized Polymers

Abstract: Phase diagrams for reversibly associating one-end-functionalized chain molecules (with an emphasis on hydrogen bonding) are determined by computer simulations of a cubic lattice model employing canonical and grand canonical Monte Carlo methods. Due to the relatively short chain lengths used, the stability of the homogeneous state is strongly enhanced compared to mean-field Random Phase Approximation predictions. Characteristic phenomenon such as reappearing phases and macrophase separation into two phases, at least one of which is microphase separated, are observed and discussed.

4.1 Introduction

Structure formation in polymer systems based on a combination of covalent bonding and reversible physical bonding such as hydrogen bonding or ionic interactions has attracted a lot of interest lately[1-14]. The phase behavior of polymer systems is dominated by the ubiquitous unfavourable interactions between unlike species. In the case of polymer blends this usually leads to undesirable macrophase separation. For block copolymers, on the other hand, this tendency may be exploited advantageously to construct well ordered nanostructures. Still, also block copolymers have the disadvantage that a usually laborious synthetic effort is required to obtain suitable molecular weights and molecular architectures. For a number of applications the combination of homopolymers or block copolymers with supramolecular chemistry offers a particularly facile concept to construct self-organized nanostructured materials with one or more characteristic length scales[15]. In recent years most of the experimental investigations focussed on comb copolymerlike structures obtained by hydrogen bonding and/or ionic bonding between homopolymers and end-functionalized oligomers (i.e. also referred to as amphiphiles or surfactants). The theoretical description of these kind of systems was initiated by Tanaka and co-workers[16]. More recently, a slightly different description was advanced in our group and used to give a detailed analysis of the ordered structures formed[17-18]. An important conclusion of both approaches is that macrophase separation, frequently involving at least one microphase separated phase, is a dominant feature in systems where bonding is reversible.

The most simple system containing block copolymerlike molecules obtained by reversible association is given by a mixture of one-end-functionalized homopolymers. An experimental example is given by a mixture of one-end-animated polystyrene and one-end-carboxylated (sulfonated) poly(ethylene glycol) investigated by Nose and co-workers[19]. Similar studies are reported by Russell et al.[20] and Iwasaki et al.[21]. All these results demonstrate that these systems behave in many ways like simple block copolymers. Theoretically, this kind of situation was already considered in the pioneering work of the group of Tanaka[22].

Here we will reconsider these mixtures of one-end functionalized polymers. Our main motivation is that the relatively simple nature of these systems offers the possibility to investigate their phase behaviour by computer simulations. In this way the predictions of the theoretical approach can be tested. The emphasis will be on the influence of fluctuation corrections, i.e. deviations from mean-field Random Phase Approximation predictions due to the relatively short chains involved, the

phenomenon of reappearing phases and macrophase separation into two phases with different or equal symmetry.

4.2 Theory

The system considered is a binary mixture of one-end-functionalized homopolymers, P(A)-X / P(B)-Y with an equal number of monomers, N, per homopolymer. The two homopolymers can reversibly associate to form a symmetric di-block copolymer by physical bonding between the functional monomers X and Y. We will consider equilibrium in an incompressible system with 1:1 associations between polymer A and B. The system consists of three different species: the free polymers and the complex between polymer A and B. This is a dynamic equilibrium so that the bonding has a finite life time. However, the species, rather than individual molecules, are still distinguishable if the number of molecules of each species remains constant. In our incompressible system, the volume fractions of the three species satisfy

$$\phi_1(T)+\phi_2(T)+\phi_{12}(T)=1 \tag{4.1}$$

where ϕ_1 and ϕ_2 are the volume fractions of *free* molecules of polymer A and polymer B respectively and ϕ_{12} is the volume fraction of *associated* molecules. The total volume fraction of polymer A and B can be expressed as

$$\begin{aligned}\phi_A &= \phi_1(T)+\frac{\phi_{12}(T)}{2}\\ \phi_B &= \phi_2(T)+\frac{\phi_{12}(T)}{2}\end{aligned} \tag{4.2}$$

Using the Flory-Huggins approximation, the free energy change of the system with ϕ_1, ϕ_2 and ϕ_{12} is given by

$$\frac{f}{k_BT}=\frac{\phi_{12}}{2N}\frac{f_a}{k_BT}+\frac{\phi_{12}}{2N}\ln\phi_{12}+\frac{\phi_1}{N}\ln\phi_1+\frac{\phi_2}{N}\ln\phi_2+\chi(\phi_1+\frac{\phi_{12}}{2})(\phi_2+\frac{\phi_{12}}{2}) \tag{4.3}$$

where f_a is the free energy change of the formation of a single association and χ is the Flory-Huggins interaction parameter between monomers A and B. For convenience we introduce φ and ψ defined by

$$\varphi(T) = \phi_1(T) + \phi_2(T)$$
$$\psi = \phi_B - \phi_A = \phi_2(T) - \phi_1(T) \tag{4.4}$$

In terms of these parameters, the free energy becomes

$$\frac{f(\varphi,\psi)}{k_BT} = \frac{1-\varphi}{2N}\frac{f_a}{k_BT} + \frac{\chi}{4}(1-\psi^2) + \frac{\varphi+\psi}{2N}\ln\frac{\varphi+\psi}{2} + \frac{\varphi-\psi}{2N}\ln\frac{\varphi-\psi}{2} + \frac{1-\varphi}{2N}\ln(1-\varphi) \tag{4.5}$$

The temperature dependency of the the volume fraction of *free* polymers φ follows from

$$\left[\frac{\partial f}{\partial \varphi}\right]_{\psi} = 0 \tag{4.6}$$

The solution of eq. (4.6) is

$$\varphi(T) = \frac{-2 + [4 + 4\mathrm{K}(T) + \mathrm{K}^2(T)\psi^2]^{1/2}}{\mathrm{K}(T)}$$
$$\mathrm{K}(T) = \exp[1 - \frac{f_a}{k_BT}] \tag{4.7}$$

The free energy change of the formation of a single associated pair, f_a, can be expressed in terms of the bonding energy and the change in entropy accompanying association,

$$\frac{f_a}{k_BT} = \frac{\varepsilon_b}{k_BT} - \frac{(s_b + s_{AB})}{k_B} \tag{4.8}$$

where ε_b is the energy of association, s_b is the entropic loss due to a loss of orientational freedom, particularly severe in the case of hydrogen bonding, and s_{AB} is the loss in configurational entropy due to linking between polymer A and B (*entropy of disorientation).* The separation of the entropy loss due to association into two contributions is not required for the theoretical analysis, however, it will be essential for a direct comparison between theory and computer simulations.

In this chapter the investigation of the phase behaviour will be restricted to the derivation of the instability boundaries, i.e. the spinodals. To find this, the structure factor S must be evaluated. Using the Random Phase Approximation[23-24], S is related to the second order vertex function Γ by

$$S = \frac{1}{\Gamma - 2\chi} \tag{4.9}$$

with

$$\Gamma = \frac{S_{AA} + S_{BB} + 2S_{AB}}{S_{AA}S_{BB} - S_{AB}^2} \tag{4.10}$$

The second order single chain correlation functions S_{ij}, appearing in this equation, are for the present system given by

$$\begin{aligned} S_{AA} &= \frac{\varphi - \psi}{2} N g_D(1,x) + 2(1-\varphi) N g_D(1/2,2x) \\ S_{BB} &= \frac{\varphi + \psi}{2} N g_D(1,x) + 2(1-\varphi) N g_D(1/2,2x) \\ S_{AB} &= (1-\varphi) N [g_D(1,2x) - 2g_D(1/2,2x)] \end{aligned} \tag{4.11}$$

Here, the scaled wave number x is defined by $x = k^2 \langle r^2 \rangle$,where k is the scattering vector and $\langle r^2 \rangle$ is the mean square radius of gyration of polymer A or B, and $g_D(f,x)$ is related to the Debye function: $g_D(f,x)=2[fx+\exp(-fx)-1]/x^2$. In the limit $x \to 0$, the vertex function Γ attains the limiting value given by

$$\Gamma(x \to 0) = \frac{4(2-\varphi)}{N(2\varphi - \varphi^2 - \psi^2)} \tag{4.12}$$

Because the vertex function in our system is temperature dependent, i.e. $\Gamma = \Gamma(x, \psi, T)$, the spinodal temperature T_s for a fixed ψ is found by solving the equations:

$$\begin{aligned} 2\chi(T_s) &= \Gamma^*(\psi, T_s) \\ \Gamma^*(\psi, T) &= \min_x \left[\Gamma(x, \psi, T)\right]_{\psi,T} \end{aligned} \tag{4.13}$$

Due to the temperature dependent association equilibrium, eq. (4.13) can only be solved by taking an expression for the interaction parameter χ in which the temperature dependence is explicitly displayed. Therefore, if it is assumed that

$$\chi = a + \frac{b}{T} \tag{4.14}$$

where a and b are constants, this leads to an expression for the spinodal condition for macrophase separation at $\psi = 0$ given by

$$a + \frac{b}{T_s} = \frac{\Gamma(0,0,T_s)}{2} = \frac{2}{N\varphi(T_s)} \tag{4.15}$$

This expression indicates that, if a solution exists (remember both the left hand side and the right hand side depend on temperature) it just corresponds to macrophase separation in a mixture of an equal number of *free* polymers A and B diluted with associated di-block copolymers (φ is the volume fraction of *free* polymers). The phase behaviour in our system is a result of the repulsive interaction between the two polymers expressed by the χ-parameter and the association strength (Eq. 4.8). If the association is weak and the repulsion strong, the system will macrophase separate. On the other hand, if the strong repulsion is combined with strong association, there will be a tendency for microphase separation. The condition for the change of the dominant fluctuation from $k^* = 0$ to $k^* \neq 0$ is found from:

$$\left[\frac{\partial\Gamma(0,\psi,T)}{\partial x}\right]_{x=0} = 0$$

$$\Leftrightarrow 3\varphi^3(T) - 14\varphi^2(T) + (20 - \psi^2)\varphi(T) - 8 = 0 \tag{4.16}$$

If the dominant fluctuation corresponds to $k^* \neq 0$ and the system is still homogeneous, the small angle scattering will show the characteristic correlation hole peak[23-24]. In the case of comb copolymerlike systems obtained by hydrogen bonding between end-functionalized oligomers and homopolymers, this has been addressed extensively in our previous papers[25-26].

4.3 Model and Simulation

To investigate the system under consideration numerically, Monte Carlo simulations with two different ensembles, grand canonical and canonical were performed. The objective of these simulations is to test several features of the theoretical predictions. In recent papers, the phase behavior of comb copolymerlike systems obtained by association between homopolymers and one-end-functionalized oligomers was addressed. These are the systems most frequently studied experimentally. The experimental systems are characterized by relatively small oligomers (15-20 carbon-carbon bonds). Also there, the theoretical modeling has been based on the mean-field Random Phase Approximation model, which strictly

speaking is only correct in the infinite chain length limit. For smaller chain lengths fluctuation corrections can in principle be calculated[27], however, even then the theory is still only valid for much longer side chains then those employed. The system studied in this chapter is the most simple one involving block copolymerlike structures obtained by reversible association. One of the main objectives of this work is therefore to compare the formally exact computer simulations with the mean-field RPA predictions. Two other characteristic features, rentrant phase behavior and macrophase separation involving one or more microphase separated phases, will also be addressed. The latter issue is of considerable interest. It is a characteristic feature of the theoretically predicted phase behaviour in associated polymer systems. However, at least for comb copolymerlike systems, it has not been observed experimentally yet. This is most likely due to the redistribution of chains required, which seems to be a very slow process.

We start by explaining the model and the simulation techniques including the model for hydrogen bonding. Two kinds of polymer chains denoted by A and B were generated on a 3-dimensional cubic lattice with a linear size of $L = 40$ (canonical) and $L = 20$ (grand canonical) expressed in units of a statistical monomer. The lattice contains 20% voids. Each polymer chain has an equal number of statistical monomers, N=16. Polymer A consists of 15 statistical monomers of type A and an end-functional monomer X and polymer B consists of 15 monomers of type B and an end-functional monomer Y. The conformations of the polymer chains are self-avoiding and mutually avoiding walks to ensure excluded volume effects. For the dispersive interaction energies ε_{ij} between statistical monomers of type i and j the simple choice of $\varepsilon_{AB} = \varepsilon_{AY} = \varepsilon_{XB} = \varepsilon$ and $\varepsilon_{AA} = \varepsilon_{BB} = \varepsilon_{XX} = \varepsilon_{YY} = 0$ was made. Since the main focus will be on hydrogen bonding as the associative interaction between the one-end-functionalized polymers, the interaction between the functional groups X and Y should be considered to have a strong directional dependency, i.e the interaction depends on the *relative* orientations of the two functional monomers (essentially a *geometrical* constraint)[28]. The number of orientations of a monomer is considered to be a large number. Since the geometry of our simple cubic lattice used for the simulations gives only two possible relative orientations, parallel and perpendicular, it is necessary to introduce a parameter q reflecting the number of possible orientations of a monomer. Let us therefore assume that each monomer has q *internal* orientational states so that the number of possible *relative* orientations between two monomers is q^2. Then we model the interaction energy as

$$\varepsilon_{XY} = \varepsilon_h \delta(c_X, c_Y) + \varepsilon[1 - \delta(c_X, c_Y)] \tag{4.17}$$

where ε_b is the energy of bonding and c_i is the variable numbering the internal states of monomer i (c_i =1,2,·····,q) and δ is the Kronecker delta function which equals unity if $c_i = c_j$ and zero otherwise. The other interactions involving the pairs AB, AY and BX are considered to be independent of these internal states. Eq (4.17) shows that only q pair states, i.e. $c_X = c_Y = 1, 2, \cdots\cdots, q$, out of all q^2 pair states have a bonding energy ε_b. In the actual Monte Carlo process, this directional specific nature of the interaction between non-bonded X and Y can be accounted for by taking

$$\varepsilon_{XY} = \begin{cases} \varepsilon_b & \text{if } \xi \le 1/q \\ \varepsilon & \text{otherwise} \end{cases} \tag{4.18}$$

where ξ is a random number uniformly distributed between zero and unity. Thus the internal states of the functional monomers X and Y are generated by a random number generator even though the simple cubic box does not have such a detailed geometry. A schematic representation of a bonded and nonbonded molecule is shown in figure 4.1.

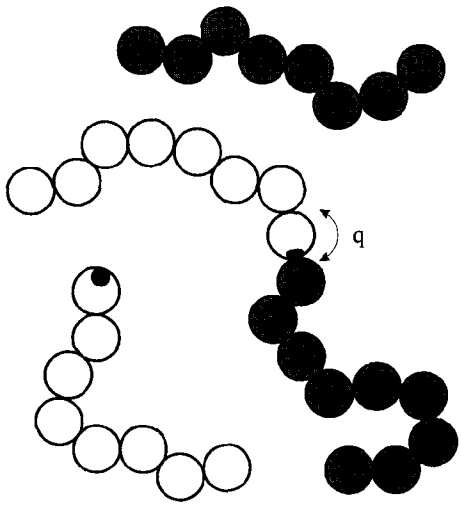

Fig. 4.1: Schematic illustration of the formation of a thermoreversible bond.

In fact, this MC process implies that each statistical monomer on the lattice also attempts to change its internal state in each Monte Carlo trial move. For all but the functional monomers, this has no effect on the interactions. Furthermore, each functional monomer can form only one hydrogen bond. There are two different

interactions in the system which will be used in the form of two interaction parameters t and r defined by

$$\frac{\varepsilon}{k_B T} = \frac{1}{t}$$
$$\frac{\varepsilon_b}{k_B T} = -\frac{r}{t} \tag{4.19}$$

so that the set of variables, $\{q, r, t\}$ is used as input for the simulations.

To sample the configurational space according to Metropolis importance sampling[29] in canonical Monte Carlo, the slithering snake algorithm[30] is used. If a randomly selected molecule is hydrogen bonded to another molecule, the slithering snake attempt is applied with probability 1/2 to the completely associated molecule: the randomly selected molecule drags the second molecule due to the hydrogen bonding. With the same probability 1/2 the slithering snake attempt is applied to the selected molecule only. Breaking and forming of a hydrogen bond can occur by slithering of one molecule, while slithering of the entire associated entity does obviously not change the number of hydrogen bonds. To calculate the structure factor at infinite wave length using the simulation box with finite size, a semi-grand canonical Monte Carlo method is performed by switching identities between polymer 1 and 2[31-32]. The transition probability for semi-grand canonical sampling is

$$W(s \to s') = \exp[\frac{n\Delta\mu}{k_B T}(\psi_{s'} - \psi_s)]\exp[-\frac{E_{s'} - E_s}{k_B T}] \tag{4.20}$$

where n is the number of polymer molecules and $\Delta\mu$ is the chemical potential difference between polymer A and B. ψ_i and E_i are the order parameter and the energy of state i respectively. The number of hydrogen bonds can of course also be changed by switching the identity of a polymer molecule. Simulations were performed with different choices of variables $\{q, r, t\}$. Quantities such as the structure factor were statistically averaged over 300 independent runs in a canonical Monte Carlo and 50000 runs in a semi-grand canonical Monte Carlo.

4.4 Results and Discussion

In this section we present the results from the simulations performed by the canonical and grand canonical Monte Carlo method and compare these with the theoretical results obtained on the basis of the Random Phase Approximation.

From the configurations simulated by canonical Monte Carlo, the numerical calculation of the structure factor is obtained by

$$S(\vec{k}) = L^{-3}\left\langle \sum_{u,v} e^{i\vec{k}\cdot(\vec{r}_u - \vec{r}_v)}\sigma(\vec{r}_u)\sigma(\vec{r}_v)\right\rangle \tag{4.21}$$

where r_i is the coordinates of site i in the simulation box and the occupation variable σ is defined by $\sigma(r) = \phi_A(r) - \phi_A$. The bracket indicates a thermodynamic average over the different configurations. Since we are mainly interested in the thermodynamic instability of the homogeneous phase, S was averaged for $|\boldsymbol{k}|=k$ so that the structure factor depends only on the modulus of $\boldsymbol{k}$. The calculation is performed as a function of temperature for a system which is characterized by $\{N, q, r, \psi\}$. The simulation data that will be presented correspond to $q = 10$ and $r = 40$ or 60. This value of q is a typical value, used before in polymer systems involving hydrogen bonding[33-34]. The values of r are within the usual range of hydrogen bonding interaction energies[35].

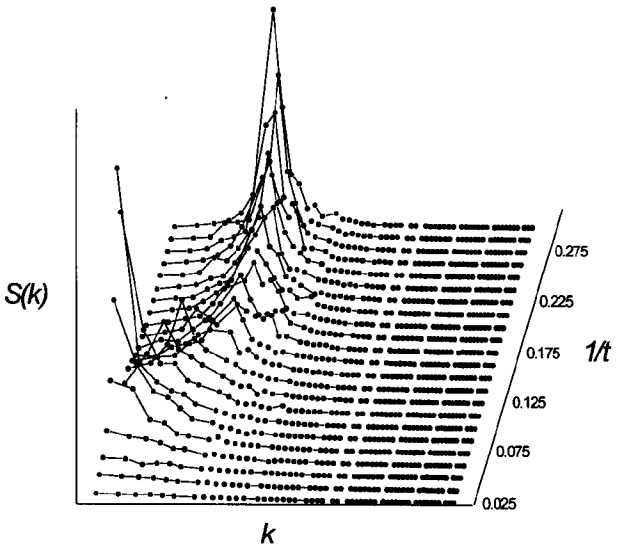

Fig. 4.2: Structure factor S(k) as a function of k and inverse temperature 1/t for the parameter set {N = 16, q = 10, r = 40, ψ = 0}.

Figure 4.2 presents the structure factors of the system for the case of $\{N = 16, q = 10, r = 40, \psi = 0\}$ as a function of the inverse temperature, $1/t$. At high temperatures, where most polymers are free, the system behaves like a simple binary mixture of

homopolymers A/B and hence $S(k)$ is a decreasing function of k. This situation changes drastically upon decreasing the temperature. Then, polymers A and B start to associate by hydrogen bonding and the system contains more associated polymers which behave like diblock copolymers. As a result, the dominant fluctuation k^* starts to shift from 0 to larger values and approaches the value corresponding to the pure diblock copolymer system. The strong increase in the value of the structure factor around $1/t \cong 0.08$ ($k \cong 0$) and $1/t \cong 0.27$ ($k^* > 0$) suggests that the system exhibits both a macroscopically and a microscopically ordered structure depending on the temperature. Of course, the phase separation at $1/t \cong 0.08$ is not guaranteed to be macrophase separation since the structure factor for wavelengths $\lambda = 2\pi/k > L$ is absent due to the finite size of simulation box. In order to clarify the behavior for this regime, a semi-grand canonical Monte Carlo simulation was performed, which allows the variation in volume fractions of polymer A and B by switching identity of A to B and vice versa. Using semi-grand canonical sampling with fixed inputs t and $\Delta\mu$, the order parameter distribution $P(\psi)$, is estimated by recording the histogram. An example of the estimated $P(\psi)$ at $1/t = 0.1125$ is shown in figure 4.3. The two peaks at $\psi = 0.85$ and -0.85 correspond to a phase coexistence in the mixture. Since the binodal points in this system, ψ' and ψ'' are symmetric around $\psi = 0$, we calculate the average order parameter by

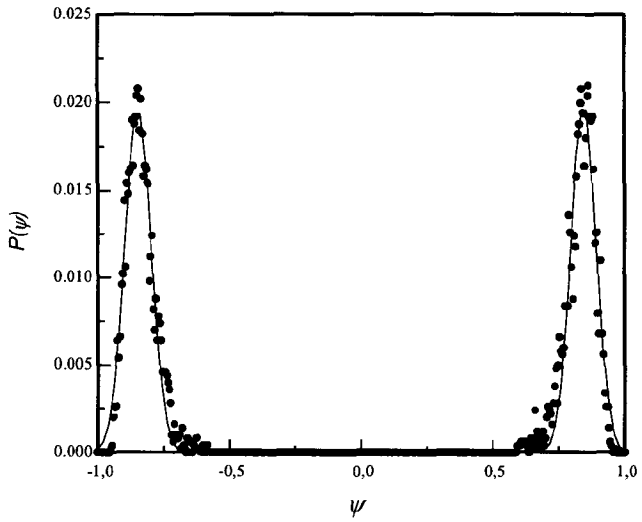

Fig. 4.3: Order parameter distribution $P(\psi)$ as a function of ψ at $1/t=0.1125$ for the parameter set {$N = 16$, $q = 10$, $r = 40$, $\Delta\mu = 0$}.

$$\langle|\psi(t)|\rangle = \sum_{\{\psi\}} |\psi| P(\psi, t) \tag{4.22}$$

Figure 4.4 presents the averaged order parameter as a function of $1/t$ for the system presented in figure 4.2. The value for $\Delta\mu$ is put to zero so that the symmetric condition, $<\psi> = 0$, is fulfilled statistically by the grand canonical sampling. Since we perform semi-grand canonical sampling with a fixed total number of polymers, n = 400, the quantity $<|\psi|>$ shows finite size effects in the range where $<|\psi|>$ is small and as a result, $<|\psi|>$ does not completely vanish in the homogeneous phase. The size independent value for $<|\psi|>$, corresponding to the binodal point ψ' can only be obtained by finite size scaling. Nevertheless, the data presented in figure 4.4 are sufficient to conclude that the strong increase in structure factor in the region $1/t \approx$ 0.07-0.125 is the result of macrophase separation. As observed in figure 4.2 and 4.4, the state of this mixture undergoes three distinctive changes by lowering the temperature, which are macrophase separation, reappearing homogeneous phase and microphase separation. The changes in morphology as a function of temperature are presented in figure 4.5 (a)-(d).

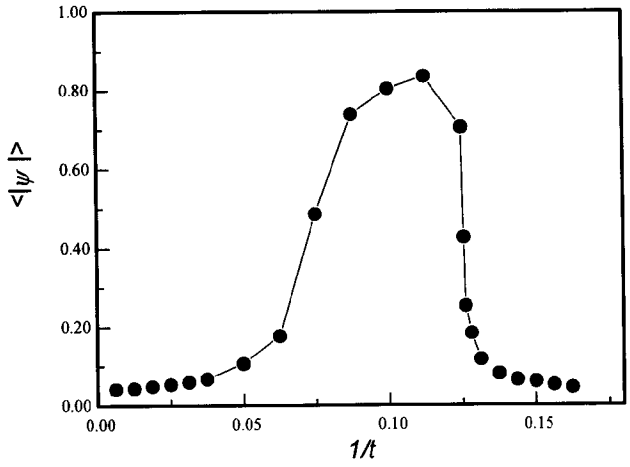

Fig. 4.4: Average order parameter $<|\psi|>$ as a function of inverse temperature 1/t for the parameter set {N = 16, q = 10, r = 40, $\Delta\mu$ = 0}.

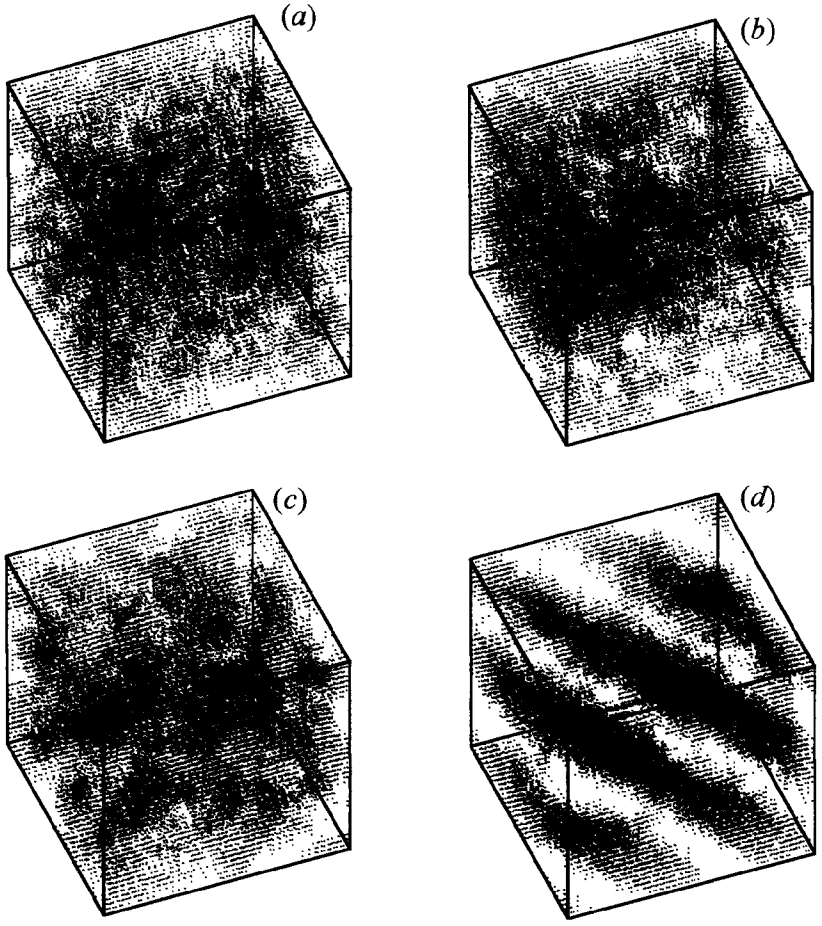

Fig. 4.5: Snapshots of the system {N = 16, q = 10, r = 40, ψ = 0}. a. 1/t = 0.025, homogeneous phase (k = 0); b. 1/t = 0.1, where the system is macrophase separated into two homogeneous phases; c. 1/t = 0.18, reappearing homogeneous phase (k* > 0); d. 1/t=0.35, where the system is microphase separated. Only one type of monomers is indicated.*

Figure 4.6 presents the same plot as in figure 4.2 but for the different case of $\{N = 16, r = 60, q = 10, \psi = 0\}$. In comparison with the previous case of $r = 40$, the hydrogen bonding strength is stronger and as a result the dominant fluctuation k^* starts to shift to larger values already at a higher temperature. It is also clear that the mixture does not undergo macrophase separation at high temperature in this case. This is due to the rapid increase in the number of associated chains preventing macrophase separation in the high temperature range.

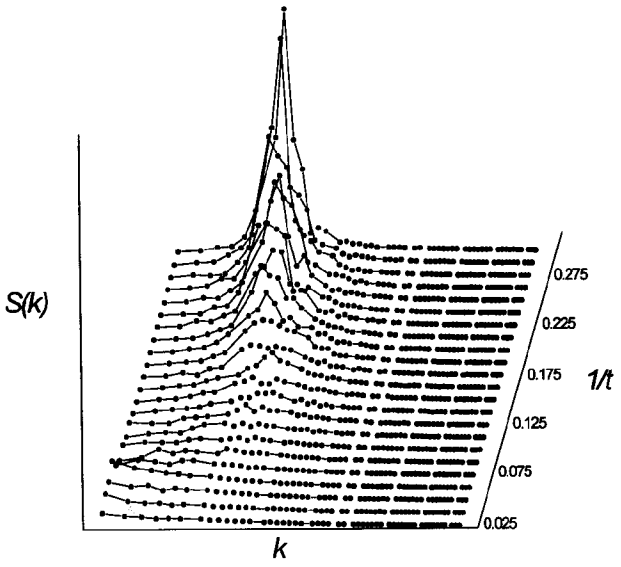

Fig. 4.6: Structure factor S(k) as a function of k and inverse temperature 1/t for the parameter set {N = 16, q = 10, r = 60, ψ = 0}.

Spinodal. Theoretically, the spinodal for macrophase separation is found by eq.(4.13). At the spinodal for $\psi = 0$,

$$\chi(t_s) = \frac{2}{N\varphi(t_s)} \tag{4.23}$$

Thus the homogeneous phase at high temperature is stable provided that

$$\chi(t) < \frac{2}{N\varphi(t)} \tag{4.24}$$

Therefore if the volume fraction of free polymer, φ, decreases rapidly by lowering the temperature so that condition (4.24) is satisfied over the entire temperature range, the mixture is completely compatibilized by associated chains, sustaining the homogeneous phase until microphase separation occurs. The temperature dependent volume fraction $\varphi(t)$ can be calculated theoretically using eq. (4.7), provided we know the free energy change of a single association between a pair of polymers, f_a. In terms of the parameters r and q, f_a, can be written as

$$\begin{aligned} \frac{f_a}{k_B T} &= \frac{\varepsilon_b}{k_B T} - \frac{(s_b + s_{AB})}{k_B} \\ &= -\frac{r}{t} - \ln\frac{1}{q} - \frac{s_{AB}}{k_B} \end{aligned} \tag{4.25}$$

The analytic expression for the entropic loss, s_{AB}, in the Flory approximation[30] is given by

$$s_{AB} = k_B \ln\frac{2(z-1)^2}{Nze} \tag{4.26}$$

where z is the coordination number. For our simulations $N = 16$ and $z = 6$ and hence

$$s_{AB} = -1.65k_B \tag{4.27}$$

Figure 4.7 presents the plot of the volume fraction of free polymers as a function of temperature for two cases. The theoretical results for each case of $\{N, q, r, \psi\}$are calculated with s_{AB} = -1.65k_B. The simulation results agree with the theoretical calculations except for the two-phase region, $1/t \approx$ 0.07-0.125, which occurs for the case of r = 40. Since the expression (4.7) is only valid in the one phase region, φ for the two phase region has to be calculated at a branch of the phase separation curve. If at temperature t the mixture for fixed ψ = 0 separates into two phases, ψ = Φ and ψ = -Φ, φ is given by

$$\varphi(t) = \frac{-2 + [4 + 4\mathrm{K}(t) + \mathrm{K}^2(t)\Phi^2(t)]^{1/2}}{\mathrm{K}(t)} \tag{4.28}$$

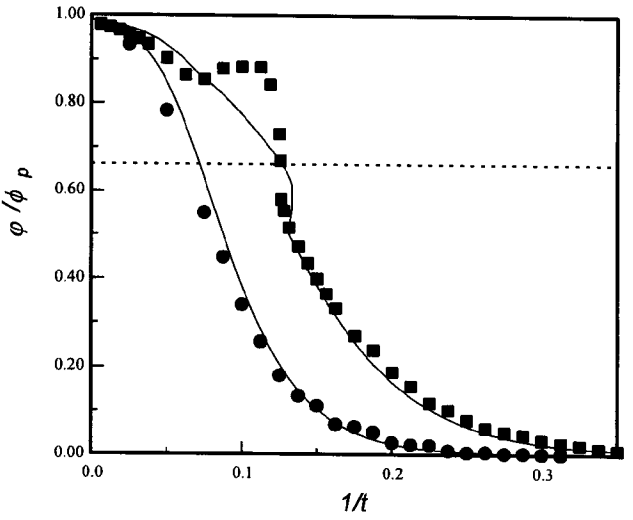

Fig. 4.7: Fraction free polymer as a function of inverse temperature 1/t for •: {N = 16, q = 10, r = 60, ψ = 0} and ■: set {N = 16, q = 10, r = 40, ψ = 0}. Solid lines represent theoretical predictions based on eq.(4.28).

The theoretical result for φ in the two phase region presented in figure 4.7 is calculated using for Φ the value at the branch of the spinodal curve. The simulation results for φ, on the other hand, correspond to the value of Φ at the branch of the binodal curve. The discrepancy between the theoretical and numerical value of free polymer in the two-phase region is believed to be partly due to the difference between spinodal and binodal. The horizontal dashed line represents the value of the critical fraction of free polymer for $\psi = 0$ and $\varphi_c = 2/3$ which is calculated by eq. (4.16). From the temperature at which φ reaches φ_c, k^* starts to shift to larger values as observed in figure 4.2 and 4.6.

In order to calculate the spinodal instability eq. (4.13), the interaction parameter χ need to be expressed as a function of temperature. As will be shown, the temperature dependence of χ turns out to be linear in $1/t$ so that

$$\chi(t) = \frac{z_{eff}}{t} \tag{4.29}$$

where z_{eff} is the effective coordination number. To determine z_{eff}, we use the following relation,

$$S^{-1}(k=0) - \Gamma(0,\psi,t) = -\frac{2z_{eff}}{t} \tag{4.30}$$

where

$$\Gamma(0,\psi,t) = \frac{4[2-\varphi(t)]}{N[2\varphi(t) - \varphi(t)^2 - \psi^2]} \tag{4.31}$$

Thus z_{eff} is determined from the slope in the plot of $[S^{-1}(k=0) - \Gamma]$ versus $1/t$. For the case of $\{N = 16, q = 10, r = 40, \psi = 0\}$, the result is presented in figure 4.8. Using the semi-grand canonical Monte Carlo method, the structure factor for $k = 0$ in figure 4.8 is estimated from the order parameter distribution, $P(\psi)$,

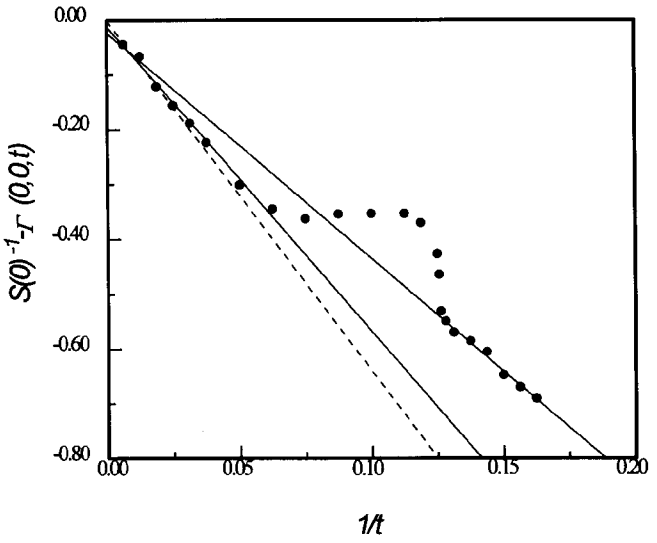

Fig. 4.8: $z_{eff}/t = S^{-1}(k=0) - \Gamma(0,\psi=0,t)$ as a function of inverse temperature 1/t for {N = 16, q = 10, r = 40, ψ = 0}. •: simulation results. Dotted line corresponds to Flory value of $z_{eff} = 3.2$. Solid lines are fits to the high temperature homogeneous regime ($z_{eff} = 2.67$) and the low temperature homogeneous regime ($z_{eff} = 2.06$).

$$S(k=0) = \frac{N^2 n^2}{4L^3}\left[\langle \psi^2 \rangle - \langle \psi \rangle^2\right] \tag{4.32}$$

The symmetric condition of $\Delta\mu = 0$, corresponding to $\psi = 0$ in the canonical ensemble, i.e. $<\psi> = 0$, is used for the calculation of eq. (4.32). Apart from the region of macrophase separation, where expression (4.30) is not valid, the plot indeed shows a linear behavior for the homogeneous regions of $1/t < 0.07$ and $1/t > 0.125$. However, the linear behavior is strikingly different in the two regimes. Our estimation of z_{eff} from the linear regression in the homogeneous region is $z_{eff} = 2.67$ for $1/t < 0.07$ and $z_{eff} = 2.06$ for $1/t > 0.125$. In fact, in the Flory lattice model χ is approximately (ignoring end effects) given by $(z\text{-}2)/t$ ($= 4/t$ for our cubic lattice). However, since 20% of the lattice sites are empty z_{eff} would be 3.2. In the Flory model, the presence of a certain monomer is uncorrelated to neighboring occupation, thereby neglecting the local correlation such as chain connectivity and the influence of the interaction with neighboring sites. In reality, the influence of the local correlation leads to a reduction of z_{eff}. In the high temperature homogeneous regime most chains are not associated and the dispersive forces are still relatively weak. Here, the reduction in z_{eff} from the Flory value of 3.2 to the actual value of 2.67 is mainly due to intramolecular correlations (cf. Ref. 36). At low enough temperatures, where $1/t > 0.125$, most chains are associated. The correlations (intra- and intermolecular) between the occupations of neighboring sites is now severely affected by the strongly unfavourable A-B interactions. Consequently, the effective coordination number for the A-B interactions is even further reduced to $z_{eff} = 2.06$.

Reappearing phases. Figure 4.9 (a) and (b) present the phase diagram obtained by the computer simulations and the spinodal phase diagram calculated from theory. The set of parameters $\{N = 16, r = 40, q = 10\}$ were used for the simulation results shown in figure 4.9a and the corresponding set of parameters $\{N = 16, r = 40, q = 10, s_{AB} = -1.65k_B, z_{eff} = 2.06\}$ were used for the theoretical result. As shown, the value of $z_{eff} = 2.06$ is valid for $1/t > 0.125$, which is the major part of the diagram. The most striking result is that the theoretical calculation of the spinodal does not show a reappearing homogeneous phase between a macrophase separated and a microphase separated regime, a property that is clearly observed in the simulation results. Of course, our determination of the phase transition for the simulation results in figure 4.9a corresponds to a first order transition whereas the theoretical calculations based on the spinodal represents a second order transition. However, this only implies that the phase separated regimes in the true theoretical phase diagram will even be larger. So, the most likely explanation, and the one we believe to be true, is that this discrepancy is due to the short chain length employed. Part of the difference might possibly be

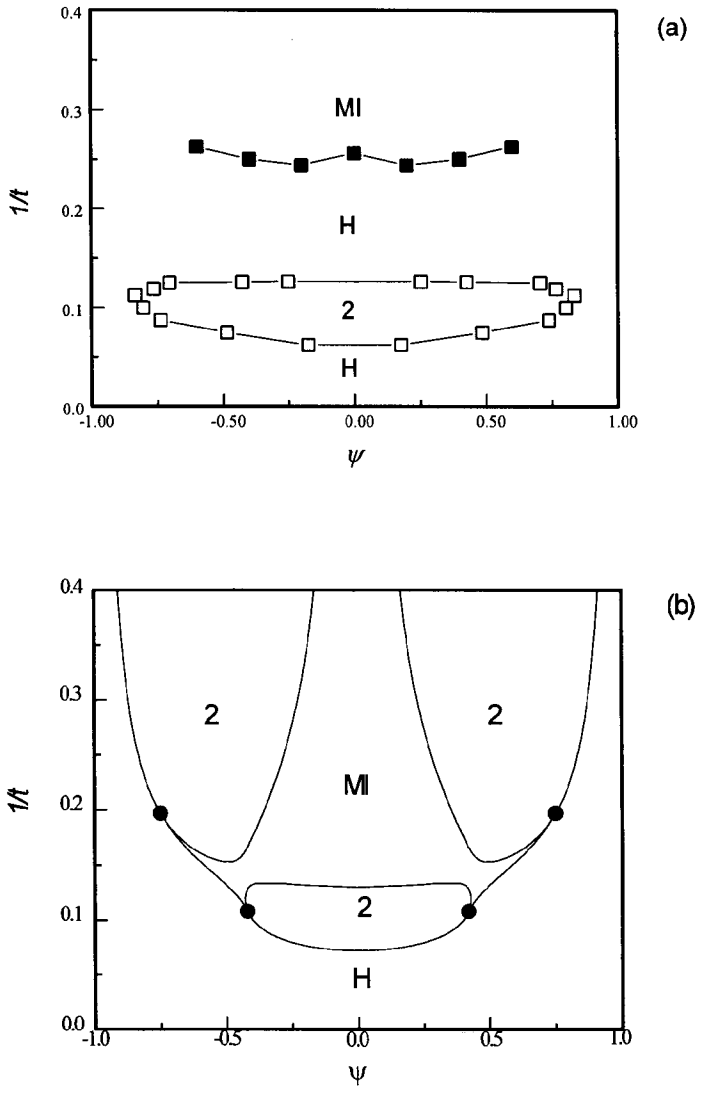

Fig.4.9: Phase diagram for {N = 16, q = 10, r = 40}. a. Determined by the simulations, □: macrophase separation, ■: microphase separation. Note high temperature region of reappearing phases b. Calculated spinodals on the basis of {N = 16, q = 10, r = 40, z_{eff} = 2.06, S_{AB} = - 1.65 k_B}. MI: one-phase microphase separated regime; 2: two-phase coexistence; •: Lifshitz points; H: homogeneous one-phase state. Note absence of high temperature reappearing phase phenomenon.

removed by applying fluctuation corrections, but it should be remembered that analytic expressions dealing with this effect are only valid for sufficiently long chain lengths[27]. By changing the values for q and r for instance to 40 and 60, keeping the other parameter values as before, the theoretical spinodal phase diagram also shows the phenomenon of reappearing phases as illustrated in figure 4.10.

Figure 4.11 presents phase diagrams for the case of r = 60 with the other parameter values as used for the results presented in figure 4.9. Both phase diagrams from simulation (figure 4.11a) and theory (figure 4.11b) show a qualitatively similar shape of the phase curve but the microphase separation temperature obtained by the simulation is again lower than the temperature of the theoretically calculated spinodal, i.e. fluctuation induced stability. The phenomenon of reappearing phases is no longer present due to the strong association already at high temperatures (relative to the dispersive interactions). To demonstrate the influence of q, spinodals have been calculated for the set of parameter values $\{r = 40, z_{ef} = 2.06, s_{AB} = -1.65\ k_B\}$. The results for the specific case of q = 1, which might be considered as representing the ionic bonding case, are presented in figure 4.12. Obviously, the phenomenon of reappearing phases, which requires bonding accompanied by an unfavourable entropy contribution, does not occur.

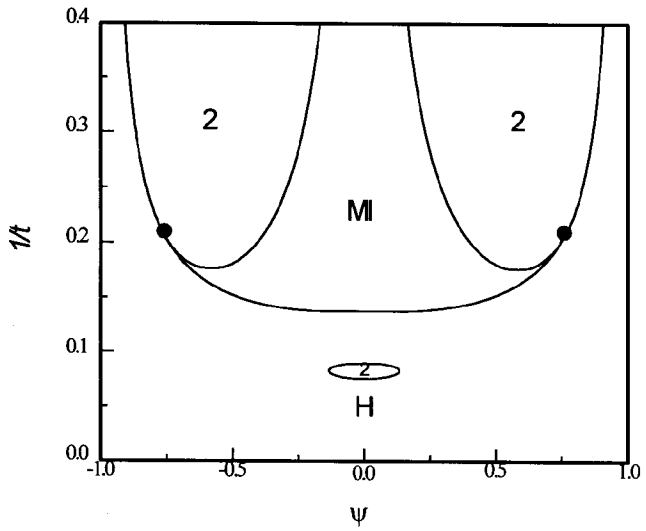

Fig. 4.10: Calculated spinodals for the parameter set {N = 16, q = 40, r = 60, z_{eff} = 2.06, S_{AB} = - 1.65 k_B} showing reappearing phase phenomenon. MI: one-phase microphase separated regime; 2: two-phase coexistence; •: Lifshitz points; H: homogeneous one-phase state.

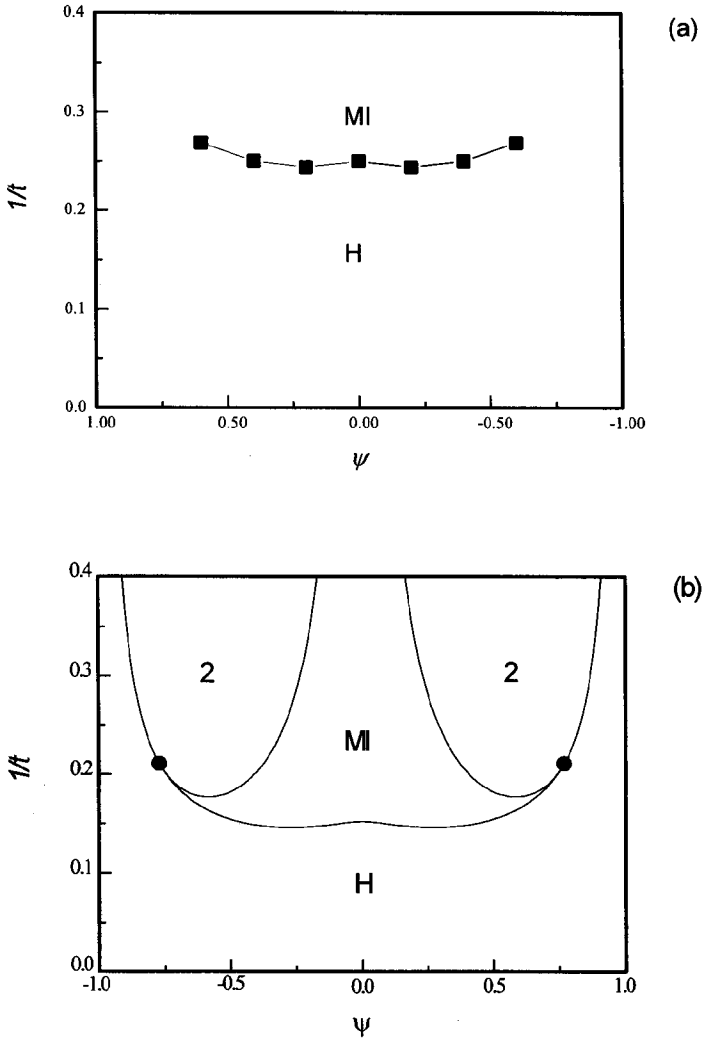

Fig. 4.11: Phase diagram for {N = 16, q = 10, r = 60}. a. Determined by the simulations, ■: microphase separation. b. Calculated spinodals on the basis of {N = 16, q = 10, r = 60, z_{eff} = 2.06, S_{AB} = - 1.65 k_B}. MI: one-phase microphase separated regime; 2: two-phase coexistence; ●: Lifshitz points; H: homogeneous one-phase state.

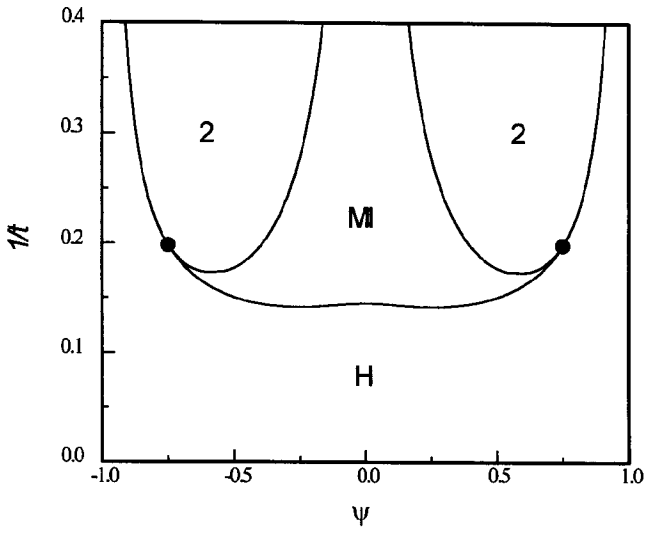

Fig. 4.12: Calculated spinodals for {N = 16, q = 1, r = 40, z_{eff} = 2.06, S_{AB} = - 1.65 k_B}. MI: one-phase microphase separated regime; 2: two-phase coexistence; •: Lifshitz points; H: homogeneous one-phase state.

Macrophase separation. An interesting feature of the theoretical calculations presented in figs 4.9-4.11 is the coexisting phases at low temperatures. For the case of {$N = 16, r = 40, q = 10, s_{AB} = -1.65k_B, z_{eff} = 2.06$}, presented in fig. 4.9, this occurs first for $1/t \approx 0.15$. At $1/t > 0.15$, the system is macroscopically separated into two microscopically ordered phases followed by phase separation into a microphase separated and a homogeneous phase for $1/t > 0.2$ (i.e. below the Lifshitz point). To address macrophase separation numerically, off-symmetric simulations have been performed for the corresponding parameter values $r = 40$ and $q = 10$ but for $\psi = 0.6$. Fig. 4.13 shows the result obtained for $1/t = 0.375$, well inside the microphase separated regime of fig. 4.9a. The figure shows the presence of two distinct lamellar phases in equilibrium with each other. The theoretical predictions also indicate the presence of a low temperature range where a homogeneous and a microphase separated phase are in equilibrium. In that regime the association is very strong, the system essentially consists of homopolymer A (60 %) and "di-block copolymer" A-B (40%) and the homopolymer is partly expelled from the lamellar phase. Our simulations have been restricted to the thermoreversible regime where the thermoreversibility of the hydrogen bonding is still probed by the computer simulations. The very strong association regime corresponds to mixtures of

homopolymers with corresponding di-block copolymers, for which the expulsion of part of the homopolymers from the lamellar structure is well known[37-38].

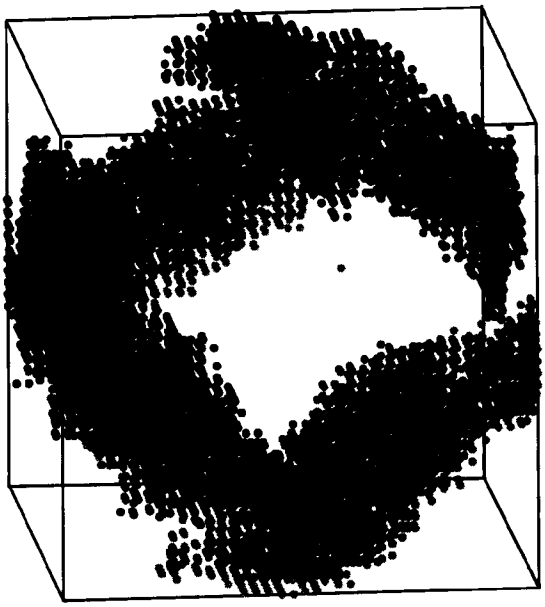

Fig. 4.13: Snapshot of macrophase separated system with phase coexistence between two microphase separated lamellar phases. {N = 16, q = 10, r = 40, ψ = 0.6, 1/t = 0.375}. Only one type of monomers indicated. The darker the monomer, the larger its z-coordinate (z-axis perpendicular to the page).

4.5 Conclusion

A computer simulation study of reversibly associating one-end-functionalized chain molecules on a cubic lattice has been presented. Phase diagrams have been determined demonstrating such characteristic phenomenon as reappearing phases and macrophase separation into phases with different symmetries. Theoretically, the phase diagrams (spinodals) have been calculated using RPA together with an effective coordination number of z_{eff} = 2.06 for the unlike dispersive interactions as determined from the low

temperature simulation data. This relatively small number for z_{eff} reflects inter- and intramolecular correlations. The phase diagram determined by the simulations shows a much larger region of stability of the homogeneously mixed state than the corresponding theoretically predicted spinodals. This is attributed to the relatively short chain lengths involved (i.e. fluctuation induced stability).

4.6 References

1. Ruokolainen, J.; ten Brinke, G.; Ikkala, O.; Torkkeli, M.; Serimaa, R. *Macromolecules* **1996**, *29*, 3409.
2. Ruokolainen, J.; Torkkeli, M.; Serimaa, R.; Komanschek, E.; Ikkala, O.; ten Brinke, G. *Phys. Rev. E* **1996**, *54*, 6646.
3. Ruokolainen, J.; Torkkeli, M; Serimaa, R.; Vahvaselkä, S.; Saariaho, M.; ten Brinke, G.; Ikkala, O. *Macromolecules* **1996**, *29*, 6621.
4. Ruokolainen, J.; Torkkeli, M.; Serimaa, R.; Komanschek, E.; ten Brinke, G.; Ikkala, O. *Macromolecules* **1997**, *30*, 2002.
5. ten Brinke, G.; Ruokolainen, J.; Ikkala, O. *Europhys. Lett.* **1996**, *35*, 91.
6. ten Brinke, G; Ikkala, O. *Trends Polym. Sci.* **1997**, *5*, 213.
7. Bazuin, C. G.; Tork, A. *Macromolecules* **1995**, *28*, 8877.
8. Kato, T.; Nakano, M.; Moteki, T.; Uryu, T.; Ujiie, S. *Macromolecules* **1995**, *28*, 8875.
9. Tal'roze, R. V.; Kuptsov, S. A.; Sycheva, T.I.; Bezborodov, V. S.; Platé, N. A. *Macromolecules*, **1995**, *28*, 8689.
10. Stewart, D.; Imrie, C. T. *Macromolecules* **1997**, *30*, 877.
11. Antonietti, M.; Burger, C.; Effing, J. *Adv. Mat.* **1995**, *7*, 751.
12. Antonietti, M.; Wenzel, A.; Thünemann, A. *Langmuir* **1996**, *12*, 2111.
13. Antonietti, M.; Burger, C.; Thunemann, A. *Trends Polym. Sci.* **1997**, *5*, 262.
14. Ober, C.; Wegner, G. *Advanced Materials* **1997**, *9*, 17.
15. Saariaho, M.; Ruokolainen, J.; Ikkala, O.; ten Brinke, G.; Torkkeli, M.; Serimaa, R.; Thomas, E. L. *Macromolecules,* submitted.
16. Tanaka, F.; Ishida, M. *Macromolecules* **1997**, *30*, 1836.
17. Dormidontova, E.; ten Brinke, G. *Macromolecules* in press.
18. Dormidontova, E.; ten Brinke, G. *Colloid and Surfaces A* in press.
19. Inomata, K.; Haraguchi, M.; Nose, T. *Polymer* **1996**, *37*, 4223.
20. Russell, T. P.; Jérôme, R.; Charlier, P.; Foucart, M. *Macromolecules* **1988**, *21*, 1709.
21. Iwasaki, K.; Hirao, A.; Nakahama, S. *Macromolecules* **1993**, *26*, 2126.
22. Tanaka, F.; Ishida, M.; Matsuyama, A. *Macromolecules* **1991**, *24*, 5582.
23. Leibler, L. *Macromolecules* **1980**, *13*, 1601.
24. de Gennes, P.G. *Scaling Concepts in Polymer Physics*; Cornell University Press: Ithaca, NY, 1979.
25. Huh, J.; Ikkala, O.; ten Brinke, G. *Macromolecules* **1997**, *30*, 1828.
26. Huh, J.; Ikkala, O.; ten Brinke, G. *Macromolecular Symposium* **1997**, *121*, 123.
27. Fredrickson, G. H.; Helfand, E. *J. Chem. Phys.* **1987**, *87*, 697.

28. Walker, J. S.; Vause, C. A. *Sci. Am.* **1987**, *256*, 90.
29. Metropolis, N.; Rosenbluth, A. W.; Rosenbluth, M.N.; Teller, A.H.; Teller, E. *J. Chem. Phys.* **1953**, *21*, 1087.
30. Wall, F. T.; Mandel, F. *J. Chem. Phys.* **1975**, *63*, 4592.
31. Sariban, A.; Binder, K. *Macromolecules* **1988**, *21*, 711.
32. Deutsch, H.P.; Binder, K. *Macromolecules* **1992**, *25*, 6214.
33. ten Brinke, G.; Karasz, F. E. *Macromolecules* **1984**, *17*, 815.
34. Sanchez, I. C.; Balazs, A. C. *Macromolecules* **1989**, *22*, 2325.
35. Jeffrey, G. A. *An Introduction to Hydrogen Bonding*; Oxford University Press: Oxford, 1997.
36. Binder, K. *Adv. Polym. Sci.* **1994**, *112*,181.
37. Whitmore, M.D.; Noolandi, J. *Macromolecules* **1985**, *18*, 2486.
38. Semenov, A. N. *Macromolecules* **1993**, *26*, 2273.